Phase Chirp Effects in Optical Clocks

An Honours Thesis

submitted in partial fulfilment of the requirements for the degree of

Bachelor of Science with Honours in Physics

presented to

the Department of Physics

Faculty of Science

National University of Singapore

A/P Murray Barrett, Supervisor

by

Cheong Cheng Wen

This Honours Thesis represents my own work and due acknowledgement is given whenever information is derived from other sources. No part of this Honours Thesis has been or is being concurrently submitted for any other qualification at any other university.

Signed: 

Acknowledgement

First, I would like to thank my supervisor A/P Murray Barrett for giving me the opportunity to work in his lab despite major renovations and his attentiveness to the progress of my project. I owe much of my learning to the kind and knowledgeable lab assistant Michael Lim, who was more than willing to troubleshoot any missteps in the experimental setup and clarify the core concepts involved. I would also like to express my gratitude for the other members of the lab (Kyle Arnold, Zhang Zhiqiang, Tan Wenyi and Bianca Lee) who have contributed theoretical insights and to the smooth progress of my project. Above all, I thank my parents and friends for their kind understanding and support.

Abstract

In an optical atomic clock, atoms or ions are interrogated by ultra-stable lasers with light pulses of specific intervals. However, the laser light needs to be switched to create interrogation pulses, and the switching of laser introduces phase chirps that register as frequency shifts in the clock atom. For this project, we investigate frequency shifts due to phase chirps from switching Acousto-Optic Modulators (AOMs) during the pulsed interrogation of clock atoms with two variables: radio-frequency (RF) power and type of interrogation (Rabi and Ramsey). We observe that the frequency shifts due to phase chirps decrease with decreasing optical power, and frequency shifts from Ramsey spectroscopy is greater than those from Rabi spectroscopy.

Contents

1. Introduction

This chapter introduces the relevant features of an optical clock for this project and explains the motivation of this project.

1.1 Optical Clocks

An optical clock is a laser stabilised to an optical cavity, with an atomic transition used as a reference frequency. Optical clocks are state-of-the-art timekeepers because they are stable and accurate.

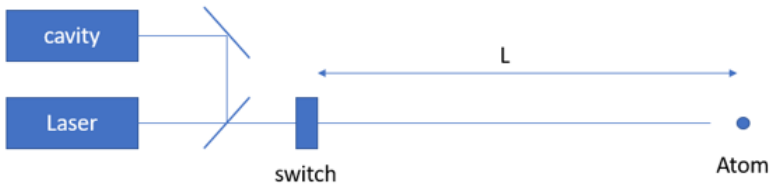

Figure 1.1: Schematic diagram of an optical atomic clock

In an atomic clock, frequency is set by oscillations of an electromagnetic field. In an optical clock, this field is provided by a laser, which is coupled to an optical cavity that serves as a ruler (frequency comb) to measure frequency with. The frequency of the laser is chosen to be near the resonance frequency of a suitable atomic transition. In clock operation, the laser repeatedly probes this atomic transition, so that we can measure and correct any frequency drifts of the cavity to maintain resonance.

In addition, we can introduce a switch that allows us to perform pulsed interrogation on the clock atom with different techniques (Rabi, Ramsey, Hyper-Ramsey). For this project, the switch used is an acousto-optic modulator (AOM), which can be used to frequency shift and compensate for path length changes as needed.

1.2 Stability and Accuracy

Stability refers to the precision by which we can measure the clock frequency. Lasers are used to interrogate an atomic transition to keep the optical clock stable. A common method is Rabi spectroscopy.

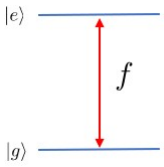

Figure 1.2: Transition frequency

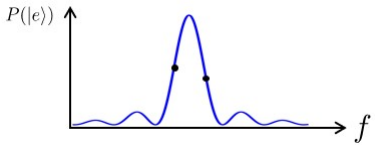

Figure 1.3: Probing the sides of a transition

The laser drives an atomic transition of frequency f from the ground to excited state (Figure 1.2) for a time T, and the population of atoms in the excited state is measured. The time T is chosen so that population transfer is maximum on resonance. If the laser frequency drifts away from resonance, the population decreases but we do not know if the frequency increased or decreased. In this scenario, we probe the atom on either side of resonance and the frequency change is inferred from the measured population (Figure 1.3).

In general, the higher the frequency domain, the better the stability of the clock. In addition, having large number of atoms and long interrogation times would also improve stability of the clock.

Accuracy refers to how well we can define the clock frequency, and can be specified by determining the effects which shift the measured atomic frequency from the unperturbed frequency. Examples of such effects are relativistic effects due to residual motion of the atom and Zeeman effect due to an external magnetic field. Accuracy can also be affected by external influences that shift the laser frequency as seen by the atom. An example would be phase chirp effects caused by changes in path length differences in the experimental setup, which can be tracked using Michelson interferometry.

1.3 Current Progress

Our group uses the singly-ionised Lutetium $^{176}Lu^{+}$ as the clock atom. Recently, we have been concerned about stability and accuracy of the clock at the low 10^{-18} s level. For example, to characterise effects that affect the accuracy of the clock, we performed precision

measurements of g-factors for the $^1S_0$ and $^3D_1$ levels, as well as the $^3D_1$ and $^3D_2$ quadrupole moments of $^{176}Lu^+$ [11]. We have also developed and experimentally demonstrated a scheme that realises hyperfine averaging during a Ramsey interrogation of the clock atom that reduces the sensitivity of the clock to its environment [6].

1.4 Outline

The stability of the clock laser needs to be maintained during its transfer from its stability-providing reference cavity to the interrogated atom. Any environmental factors that affect the atomic transition or laser frequency as seen by the atom influence the accuracy of the clock. For this project, we are interested in the path length changes between the point at which the laser is stabilised (i.e. cavity) and where the atom is probed. Any path length changes will represents a phase shift, which will be seen by the atom as a frequency shift.

The issue with switching AOMs is that it causes a phase chirp in the first-order diffracted laser beam, which translates to a frequency shift during the interrogation of an atom. A recent paper[9] has given a relative frequency shift of below 2×10^{-17} after switching on the AOM and phase lock. In order to achieve 10^{-19} precision in our clock, we need to take care of every step which can induce additional error in the laser and frequency measurements.

This project investigates two factors underlying phase chirp effects due to switching AOMs: RF power driving the AOM and interrogation techniques (Rabi and Ramsey).

2. Background

This chapter explains the ideas on which the project is based on and how phase is measured in the setup.

2.1 Acousto-Optic Modulator

An AOM is an optical device that diffracts and shifts the frequency of light using sound waves at radio-frequency.

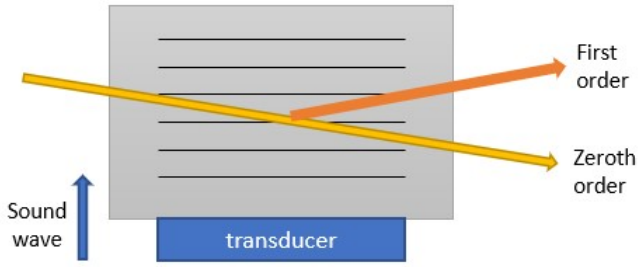

Figure 2.1: Schematic of an AOM

There are two components to an AOM: a solid crystal and a transducer. The transducer is driven by an oscillating electric signal, which creates acoustic waves in the crystal. The row of atoms in the crystal expand and contract periodically according to the driving frequency, which translates to a change in reflective index. Incoming light scatters off the rows of crystal atoms and forms an interference pattern similar to those under Bragg diffraction, which is given by[2]:

$$2\omega_{rf} \sin\theta = m\frac{\lambda}{n} \tag{2.1}$$

where ω_{rf} is the driving frequency, θ is the angle of incidence on the transverse plane of the crystal, m is the order of diffraction, n is the reflective index of crystal, and λ is the wavelength of the incident light. In the operations of an optical clock, only the zeroth and first order ($m = +1$) are of concern, and the first order diffraction is what we use to

interrogate the clock atom.

As a result of diffraction, the frequency of the first-order beam f_1 is Doppler shifted:

$$f_1 = f_0 + \gamma \tag{2.2}$$

where f_0 denotes the frequency of the zeroth-order beam.

We can also determine the diffraction efficiency at first order η due to AOM switching by taking the ratio of the optical power of the first-order diffracted beam I_1 and that of input beam I:

$$\eta = \frac{I_1}{I} \tag{2.3}$$

As an experimental benchmark, we want to maximise the diffraction efficiency at first order η of all AOMs in the setup. The next thing we need is a method to capture phase data so that the phase chirp can be observed.

2.2 Michelson Interferometry

Interferometry is an experimental technique which uses interference of superimposed waves. A Michelson interferometer is a configuration of a beamsplitter and two mirrors gives an interference pattern based on path length difference in the detector[8].

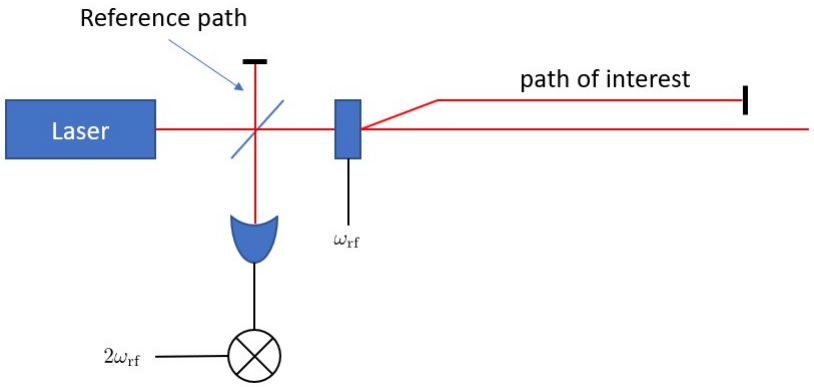

Figure 2.2: Schematic of a Michelson Interferometer

The laser first meets the beamsplitter and splits into two perpendicular paths. The reference path is short relative to the other path and assumed to be phase stable. The other path meets the AOM driven by a frequency ω_{rf} and gets diffracted into its zeroth and first

order. The first order path proceeds towards the clock atom, while the zeroth order path gets reflected meets a mirror and gets reflected back to the beamsplitter. Here, the reflected beam in the path of interest is frequency shifted twice.

Both reflected light from the reference path and the path of interest forms an interference pattern at the detector, which we call a beat note. Any phase shifts due to path length changes will be seen as a frequency shift relative to a stable RF reference at the detector, and can be compensated by changing ω_{rf}.

We can describe this process mathematically as well. Suppose we have a light beam characterised by the exponential waveform:

$$\tilde{E}_0 = E_0 \ \exp[i(kx - \omega t + \phi)] \tag{2.4}$$

where E_0 is the maximum amplitude of the wave, k is its wavenumber, x is the distance travelled by the wave, ω is its angular frequency and ϕ is its phase. Suppose that the reference path is of length L_1, and the path of interest of length L_2. We can express the waveform for the reference path as:

$$\begin{aligned} E_1 &= \frac{E_0}{2} \ \exp[i(k(x + 2L_1) - \omega t + \phi] \\ &= \frac{\tilde{E}_0}{2} \ \exp(i2kL_1) \end{aligned} \tag{2.5}$$

and the waveform for the path of interest as:

$$\begin{aligned} E_2 &= \frac{E_0}{2} \ \exp[i(k(x + 2L_2) - (\omega + 2\omega_{rf})t + \phi] \\ &= \frac{\tilde{E}_0}{2} \ \exp[i2(kL_2 - \omega_{rf} t)] \end{aligned} \tag{2.6}$$

When they meet at the detector, the amplitude of their superposition gives:

$$\begin{aligned} |E_1 + E_2|^2 &= |E_1|^2 + |E_2|^2 + 2\,\mathrm{Re}(E_1 E_2^*) \\ &= \tilde{E}_0^2 \ [1 + \cos 2(k|L_1 - L_2| + \omega_{rf} t)] \\ &= \tilde{E}_0^2 \ [1 + \cos 2(k\Delta x + \omega_{rf} t)] \end{aligned} \tag{2.7}$$

where we denote the path difference is $\Delta x = |L_1 - L_2|$, which is related to the phase difference $\Delta\phi$:

$$\Delta\phi = \frac{2\pi}{\lambda}\Delta x \tag{2.8}$$

Essentially, any changes in phase of the beat note due to changes in path difference can be compensated for by adjusting the driving frequency of the AOM ω_{rf}.

Since we want to characterise phase chirp effects resulting from the switching of AOMs, we need another device that computes and registers the phase of the beat note at the end of the interferometer.

2.3 I/Q Demodulation

To measure phase shifts resulting from the switching of AOMs, we use a universal software radio peripheral (USRP), which is a software-defined radio that performs in-phase/quadrature (I/Q) demodulation[7].

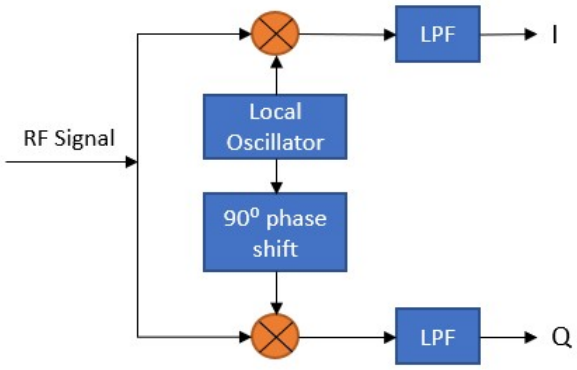

Figure 2.3: Circuit diagram of an I/Q demodulator

From the photodetector, the beat note passes through an analog output device and converts it into a RF signal. From the left of Figure 2.3, the RF signal is split into two paths. One path is directly multiplied with a reference in-phase signal (I) to produce a beat signal, while the other multiplied by a $\frac{\pi}{2}$ phase-shifted quadrature signal (Q). Both resultant beat signals are passed through low pass filters (LPF), which removes the high-frequency content that are present after multiplication of signals.

Effectively, I/Q demodulation splits the beat note into two orthogonal components that are $\frac{\pi}{2}$ out of phase. If we have a signal that has the waveform of $A_0 exp[i(\omega t + \phi)]$, we have the I and Q components as:

$$\begin{aligned} I(t) &= A_0 \ \exp[i(\omega t + \phi)] \ exp(-i\omega t) \\ &= A_0 \ \exp(i\phi) \\ &= A_0(\cos\phi - i\sin\phi) \end{aligned} \tag{2.9}$$

$$\begin{aligned} Q(t) &= A_0 \ \exp[i(\omega t + \phi)] \ \exp\Big[-i(\omega t + \frac{\pi}{2})\Big] \\ &= A_0 \ \exp\Big[i(\phi - \frac{\pi}{2})\Big] \\ &= A_0 \ (\sin\phi - i\cos\phi) \end{aligned} \tag{2.10}$$

where ω is the angular frequency of the RF signal and ϕ is the phase shift incurred along the laser path. We can easily calculate ϕ and A_0 at any time t by trigonometry:

$$\phi = \tan^{-1}[\frac{\mathrm{Re}[Q(t)]}{\mathrm{Re}[I(t)]}]$$

$$A_0 = \sqrt{[\mathrm{Re}[Q(t)]]^2 + [\mathrm{Re}[I(t)]]^2}$$

Once we have acquired phase data of AOM switching through the USRP, we need a theoretical framework to understand how a phase chirp translates to a frequency chirp when seen by the atom.

3. Theory

This chapter reviews the theoretical basis of this project and explains how frequency shifts are calculated from phase chirps.

3.1 Bloch Sphere

To understand how clock interrogation works, it is convenient to use a geometric representation of the atom's state. For a two-level system, the time-independent Hamiltonian under rotating wave approximation is given by[5]:

$$H = -\frac{\hbar}{2}\begin{pmatrix} \Delta & \Omega \\ \Omega^* & -\Delta \end{pmatrix} \tag{3.1}$$

where Δ is the detuning of the laser and Ω is the Rabi frequency, which is the transition dipole moment projected onto the electric field amplitude.

In general, the state of a two-level atom can be written as a superposition of ground and excited state[5]:

$$|\psi\rangle = c_g\,|g\rangle + c_e\,|e\rangle$$

We can define three useful components of a state vector $\mathbf{x}$:

$$x_1 = 2\,\mathrm{Re}(c_e c_g^*) \tag{3.2}$$

$$x_2 = 2\,\mathrm{Im}(c_e c_g^*) \tag{3.3}$$

$$x_3 = |c_e|^2 + |c_g|^2 \tag{3.4}$$

which satisfies the normalisation condition:

$$\sum_k |x_k|^2 = (|c_e|^2 + |c_g|^2)^2 = 1 \tag{3.5}$$

Any state $|\psi\rangle$ can be described as a point on a unit sphere known as Bloch sphere. To track how the state of an atom evolves over time on the Bloch sphere, we first solve the

Schrodinger equation using the two-level Hamiltonian and obtain the time derivative of c_e and c_g:

$$\dot{c_g} = \frac{i}{2}(\Delta c_e + \Omega c_g) \tag{3.6}$$

$$\dot{c_e} = \frac{i}{2}(\Omega^* c_e - \Delta c_g) \tag{3.7}$$

We can take the derivative of the three components and substitute the above expressions accordingly to obtain:

$$\dot{x_1} = \mathrm{Im}(\Omega)x_3 - \Delta x_2 \tag{3.8}$$

$$\dot{x_2} = -\mathrm{Re}(\Omega)x_3 + \Delta x_1 \tag{3.9}$$

$$\dot{x_3} = \mathrm{Re}(\Omega)x_2 - \mathrm{Im}(\Omega)x_1 \tag{3.10}$$

We can summarise the motion of the state vector $\mathbf{x}$ on the Bloch sphere with:

$$\dot{\mathbf{x}} = \mathbf{\Omega} \times \mathbf{x} \tag{3.11}$$

where $\mathbf{\Omega} = (\mathrm{Re}(\Omega), \mathrm{Im}(\Omega), \Delta)$. Equation (3.11) describes an anti-clockwise precession of the state vector $\mathbf{x}$ about the direction of $\mathbf{\Omega}$. In effect, we can describe the sequence of a clock interrogation as a series of rotations on the Bloch sphere.

3.2 Interrogation Techniques

During clock operation, the atomic state is usually kept at the full width at half maximum (FWHM) point (i.e. 50% at ground state, 50% at the excited state) since the atomic population is most sensitive to changes of the laser frequency seen by the atom. If there are changes to the population away from the FWHM, we need to know whether the laser frequency seen by the atom has increased or decreased so that we can compensate for these changes through the setup. To do so, we need controlled ways of interrogating the atom, and the two most common technique is called the Rabi and Ramsey spectroscopy.

3.2.1 Rabi Spectroscopy

Spectroscopy refers to the study of interaction between light and matter as a function of the light's frequency. A Rabi cycle is a continuous oscillation of an atomic state between two energy levels (e.g. ground to excited, excited to ground) in the presence of a driving field.

In Rabi spectroscopy, a laser beam with a frequency close to the resonance frequency drives atomic population from one state to the other for some interrogation time T. The difference between the resonance frequency and the laser frequency is called the detuning Δ. If the detuning is zero, the population flips entirely (i.e. 100% ground to 100% excited, vice versa). When the detuning is non-zero, the response of the atom decreases as detuning increases.

The Rabi π pulse on resonance can be visualised on a Bloch sphere as:

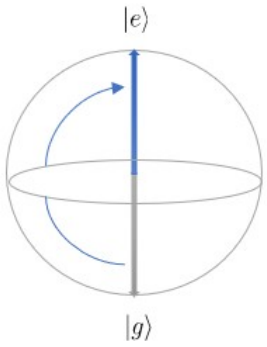

Figure 3.1: Bloch sphere representation of a Rabi π pulse

where the atom moves from a ground state $|g\rangle$ (grey arrow) to an excited state $|e\rangle$ (blue arrow).

The probability of finding the atom in an excited state with Rabi spectroscopy is:

$$P(e) = \frac{\Omega^2}{\Omega^2 + \Delta^2} \sin^2\left(\frac{T}{2}\sqrt{\Omega^2 + \Delta^2}\right) \tag{3.12}$$

where Ω is the laser frequency and T is the interrogation time.

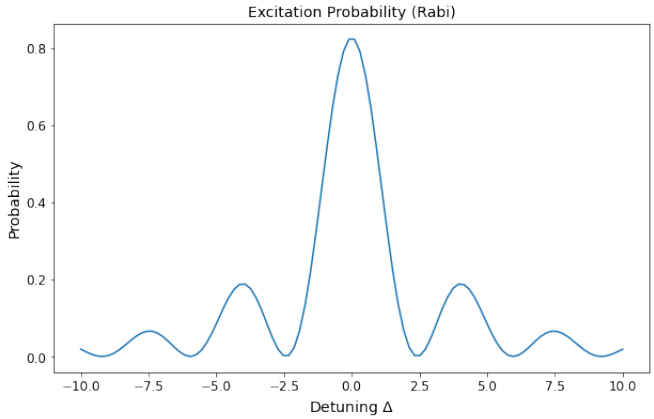

Figure 3.2: Plot of the Rabi excitation probability with $T = 1$ and $\Omega = 2$

In clock operation, the laser frequency is usually chosen such that half of the atomic population is excited, which means that the detuning Δ is set at the half width at half maximum (HWHM). The HWHM can be found by solving equation (3.12) for Δ at $P(e) = 0.5$, which is given by $\pm 0.399343/T$ in literature[3].

3.2.2 Ramsey Spectroscopy

Instead of having a long interaction time of the laser with the atom, we can opt for two short pulses with a long waiting time in between. The Ramsey sequence is essentially equivalent to a Rabi π pulse broken into two short $\frac{\pi}{2}$ pulses of time t_p, with long dead time T_d in between, with the second pulse phase shifted by $\frac{\pi}{2}$ (otherwise the pulse has no effect on the atomic state). The advantage of this approach is that the atom is less susceptible to frequency drifts from the laser due to the much shorter interaction time, hence an improved precision in determining Δ.

On the Bloch sphere, the Ramsey $\frac{\pi}{2} - T_d - \frac{\pi}{2}$ sequence with a small detuning can be visualised as:

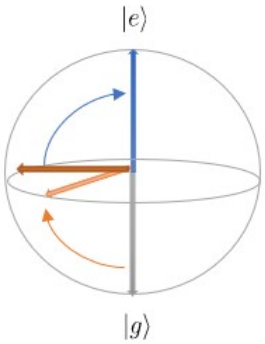

Figure 3.3: Bloch sphere representation of a Ramsey $\frac{\pi}{2} - T_d - \frac{\pi}{2}$ pulse

where the atom moves from a ground state (grey arrow) to the equatorial plane (orange arrow), precesses about the z-axis due to the detuning Δ for a dead time T_d, and moves to the final state (blue arrow). When $\Delta = 0$ (at resonance), the precession does not occur and the atom moves to the excited state, similar to a Rabi π pulse on resonance.

The probability of finding the atom in an excited state with Ramsey spectroscopy close to resonance is:

$$P(e) = \cos^2(\frac{\Delta T_d}{2}) \tag{3.13}$$

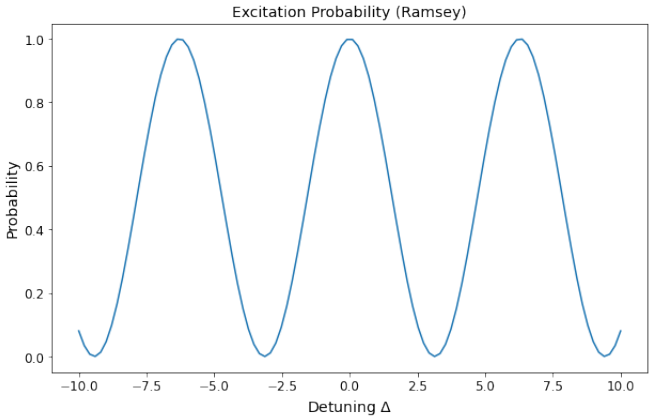

Figure 3.4: Plot of the Ramsey excitation probability with $T_d = 1$

Solving equation (3.13) for the detuning at HWHM gives us $\Delta = \frac{\pi}{2T_d}$.

3.2.3 Hyper-Ramsey

In order to combat excitation-related frequency shifts (e.g. a.c. Stark shift) of clock transition during the long dead time T_d of the Ramsey sequence, additional $\frac{\pi}{2}$ pulses can be added after T_d to reduce sensitivity. This enhanced scheme is called the Hyper-Ramsey sequence[10]. A mathematical explanation of how Hyper-Ramsey reduces excitation-related frequency shifts is found in Appendix A.

On the Bloch sphere, the Hyper-Ramsey $\frac{\pi}{2} - T_d - \frac{3\pi}{2}$ sequence with a small detuning can be visualised as a full 2π rotation about the y-axis:

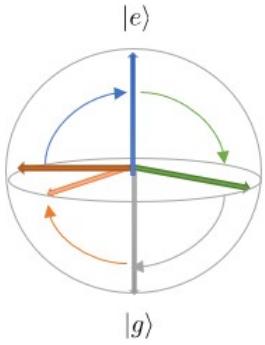

Figure 3.5: Bloch sphere representation of a Hyper-Ramsey $\frac{\pi}{2} - T_d - \frac{3\pi}{2}$ sequence

The probability of finding the atom in an excited state with Hyper-Ramsey (assuming Δ is close to resonance) is:

$$P(e) = \sin^2(\frac{\Delta T_d}{2}) \tag{3.14}$$

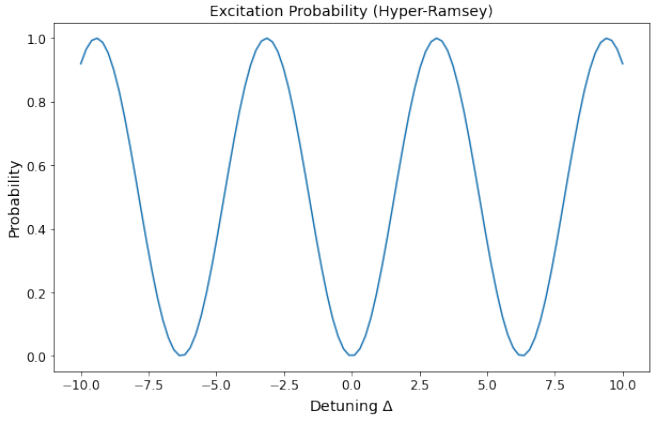

Figure 3.6: Plot of the Hyper-Ramsey excitation probability with $T_d = 1$

Solving equation (3.14) for the detuning at HWHM also gives us $\Delta = \frac{\pi}{2T_d}$.

3.3 Sensitivity Function

In order to estimate the frequency shift as seen by the atom due to a phase chirp for each interrogation technique, we need to first estimate how a change in phase relates to a small change in excitation probability δp during clock interrogation.

One method that estimates Δp in a two level system is the use of a sensitivity function [3]. The sensitivity function is a response of the measured excitation probability at the end of an interrogation due to a small step jump in frequency $\delta\nu$ at an instantaneous time t, described by a delta function. Consequently, the total change in excitation probability to a small, time-varying frequency fluctuation over the total pulse time T is given by:

$$\delta p = \frac{1}{2}\int_0^T 2\pi\delta\nu(t)\cdot g(t)dt \tag{3.15}$$

where $\phi(t)$ is the phase jump at time t. The factor of $\frac{1}{2}$ is a matter of mathematical convenience.

Since frequency is given by the time derivative of instantaneous phase (i.e. $\delta\nu(t) = \frac{1}{2\pi}\frac{d}{dt}\phi(t)$), we can also describe the change in excitation probability as a small step jump in frequency at time t. Using integration by parts on equation (3.15),

$$\delta p = \frac{1}{2}[\phi(t)\cdot g(t)]_0^T - \frac{1}{2}\int_0^T \phi(t)\cdot\frac{d}{dt}g(t)dt \tag{3.16}$$

$$= -\frac{1}{2}\int_0^T \phi(t)\cdot\frac{d}{dt}g(t)dt \tag{3.17}$$

The first term in equation (3.16) cancels off since the exact integral of $g(t)$ over the total pulse time T is zero. What remains in equation (3.17) is the second term, which says that we can calculate δp by numerically integrating the product of $\phi(t)$ and the time derivative of the sensitivity function $\frac{d}{dt}g(t)$ at each instance t over total pulse time T.

To calculate the frequency shift given a change in excitation probability, we assume the excitation probability is described by a Lorentzian lineshape with a peak excitation probability p_{max}[9]. At the half maximum points, the slope of the Lorentzian is $\pm\frac{1}{2}$. Since

the change in excitation probability happens at both sides of resonance with opposite signs (i.e. $\Delta p = 2\delta p \cdot p_{max}$), a difference Δp of the two excitation probabilities at the half maximum points leads to a resultant frequency shift of:

$$\Delta\nu = \frac{\Delta p}{2 \cdot p_{max}} \text{FWHM} \tag{3.18}$$

$$= \delta p \cdot \text{FWHM} \tag{3.19}$$

where FWHM is the full width at half maximum.

The form of $g(t)$ depends on the type of pulse used (Rabi, Ramsey or Hyper-Ramsey). We will now look at how each of the three sensitivity functions are derived.

3.3.1 Rabi Pulse

To derive the Rabi sensitivity function, let a laser beam of frequency ω_π meet the atom with a resonance frequency ω_0. We can represent this interaction with a frequency diagram[3]:

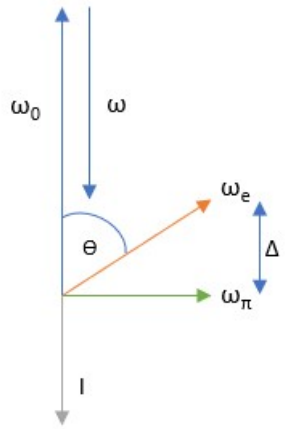

Figure 3.7: Frequency diagram with initial state vector I in a rotating reference system

where $\Delta = \omega_0 - \omega$ is the detuning. For convenience, we define ω_0 as the positive z-axis (blue arrow) and I the negative z direction. The amplitude of the Rabi π pulse lies in the positive x-axis (green arrow), which produces an effective frequency ω_e in the y-axis (orange arrow). Let θ be the angle between the resonance frequency ω_0 and the effective frequency ω_e.

We choose a laser amplitude ω_π that completely inverts the population with an interrogation time T:

$$\omega_\pi = \frac{\pi}{T}$$

Using Euler matrices for solid body rotations:

$$r_z(\theta) = \begin{pmatrix} cos\theta & sin\theta & 0 \\ -sin\theta & cos\theta & 0 \\ 0 & 0 & 1 \end{pmatrix}$$

$$r_y(\theta) = \begin{pmatrix} cos\theta & 0 & -sin\theta \\ 0 & 1 & 0 \\ sin\theta & 0 & cos\theta \end{pmatrix}$$

We can define a rotation operator:

$$rot(\theta, \alpha) = r_y(\theta) r_z(\alpha) r_y(-\theta) \tag{3.20}$$

which generates a rotation by an angle α about the effective frequency ω_e.

With state vector I initially facing down, we can express θ as a function of Δ:

$$\begin{aligned} \theta(\Delta) &= \frac{\pi}{2} + \tan^{-1}(\frac{\Delta}{\omega_\pi}) \\ &= \frac{\pi}{2} + \tan^{-1}(\frac{\Delta T}{\pi}) \end{aligned}$$

For a π pulse, the total angle Ω over which rotation takes place is:

$$\Omega(\Delta) = \pi\sqrt{1 + (\frac{\Delta T}{\pi})^2} \tag{3.21}$$

The net difference in population between the ground and excited state is given by the z-component of this rotation:

$$n(\Delta) = \begin{pmatrix} 0 \\ 0 \\ 1 \end{pmatrix}^T rot(\Delta, \Omega(\Delta)) \begin{pmatrix} 0 \\ 0 \\ -1 \end{pmatrix}$$

The sensitivity $g(t)$ of $n(\Delta)$ at time t after the pulse begins can be described in three steps: a partial rotation of I about ω_e corresponding to the time before the phase shift, followed by an infinitesimal rotation $\delta\phi$ about the z-axis due to the phase shift, and another partial rotation after the shift that completes the interrogation. In essence:

$$g(t) = lim_{\delta\phi \to 0} \begin{pmatrix} 0 \\ 0 \\ 1 \end{pmatrix}^T rot(\theta, \Omega_2(t))\ r_z(\delta\phi)\ rot(\theta, \Omega_1(t)) \begin{pmatrix} 0 \\ 0 \\ -1 \end{pmatrix}$$

For the case of a Rabi π pulse, this expression reduces to:

$$g(t) = \sin^2\theta\ \cos\theta \times [(1 - \cos(\Omega_2))\ \sin(\Omega_1) + (1 - \cos(\Omega_1))\ \sin(\Omega_2)] \tag{3.22}$$

where

$$\Omega_1 = \Omega\frac{t}{T}$$
$$\Omega_2 = \Omega(1 - \frac{t}{T})$$

The plot of $g(t)$ against time t is:

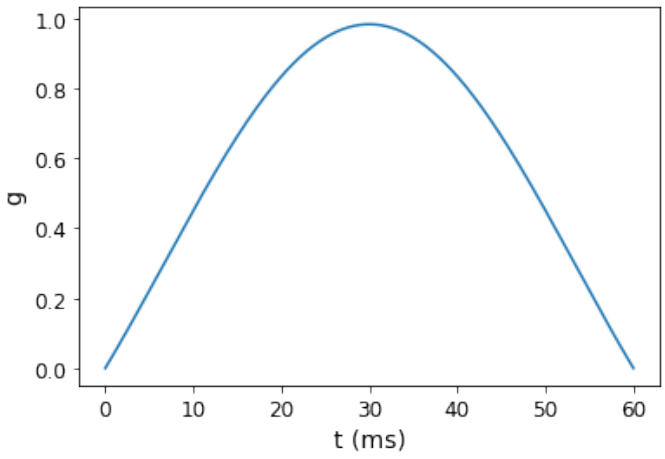

Figure 3.8: Rabi sensitivity $g(t)$ against time t for a 60 ms π pulse

which confirms the existing results in literature[3][9]. The atomic population is the most sensitive to change in at $g = 1$ and least so at $g = 0$. The atomic state at $g = 1$ corresponds to an equal superposition of the ground and excited states (i.e. half in ground, half in excited), while at $g = 0$ it is either entirely at the ground or excited state.

The derivative of the Rabi sensitivity function $\frac{d}{dt}g(t)$ is:

$$\frac{d}{dt}g(t) = \frac{2\pi\Delta}{1+(2T\Delta)^2} \cdot [(1-\cos\Omega_2)\cos\Omega_1 - (1-\cos\Omega_1)\cos\Omega_2] \tag{3.23}$$

The plot of $\frac{d}{dt}g(t)$ against time t is:

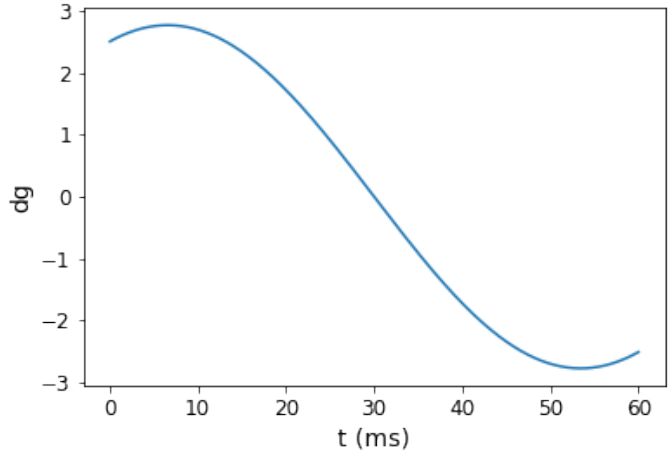

Figure 3.9: Time derivative of the Rabi sensitivity $\frac{d}{dt}g(t)$ against time t for a 60 ms π pulse

As the time scale of the phase chirp we observe is about 0.05 ms, only the first half of the first curve of $\frac{d}{dt}g(t)$ is of concern.

3.3.2 Ramsey Pulse

We repeat a similar calculation for the Ramsey $\frac{\pi}{2} - T_d - \frac{\pi}{2}$ pulse to obtain its sensitivity function $g(t)$. Since the pulse can be separated into three distinct parts, the derivation of $g(t)$ for the Ramsey sequence is much simpler. Namely, the rotation operator $rot(\theta)$ is simply $r_y(-\theta)$ for the first pulse and $r_y(\theta)$ for the second pulse. Note that the second pulse is phase shifted by $\frac{\pi}{2}$. $\theta(t)$ is the angle between the z axis and the xy-plane that goes from 0 to $\frac{\pi}{2}$ within the pulse time t_i.

$$g(t) = \begin{cases} \sin\left(\frac{\pi}{2} \cdot \frac{t}{t_i}\right) & \text{for } 0 \leq t < t_i \\ 1 & \text{for } t_i \leq t < T_d + t_i \\ \cos\left(\frac{\pi}{2} \cdot \frac{t - T_d - t_i}{t_i}\right) & \text{for } T_d + t_i \leq t < T_d + 2t_i \end{cases} \tag{3.24}$$

where t_i is the pulse time of the each of the $\frac{\pi}{2}$ pulses and T_d is the dark time.

The plot of $g(t)$ against time t is:

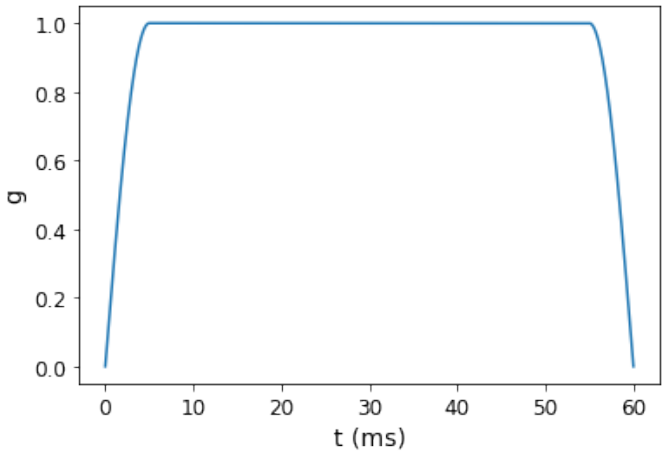

Figure 3.10: Ramsey sensitivity $g(t)$ against time t for two 5 ms $\frac{\pi}{2}$ pulses and $T_d = 50$ ms

The dark time T_d is the period where $g(t) = 1$, which means that the atomic state is in an equal superposition of ground and excited states. On a Bloch sphere, we can visualise this as a precession about the z-axis on the equatorial xy-plane due to the detuning.

Note that the results we derived here are different from the ones given in literature[3][9]. The Ramsey sensitivity function in both sources produce plots of $g(t)$ that differ from the intended shape.

The time derivative for the Ramsey sensitivity function is:

$$\frac{d}{dt}g(t) = \begin{cases} \frac{\pi}{2t_i} \cos\left(\frac{\pi}{2} \cdot \frac{t}{t_i}\right) & \text{for } 0 \leq t < t_i \\ 0 & \text{for } t_i \leq t < T_d + t_i \\ -\frac{\pi}{2t_i} \sin\left(\frac{\pi}{2} \cdot \frac{t - T_d - 2t_i}{t_i}\right) & \text{for } T_d + t_i \leq t < T_d + 2t_i \end{cases} \tag{3.25}$$

with the plot of $\frac{d}{dt}g(t)$ against time t:

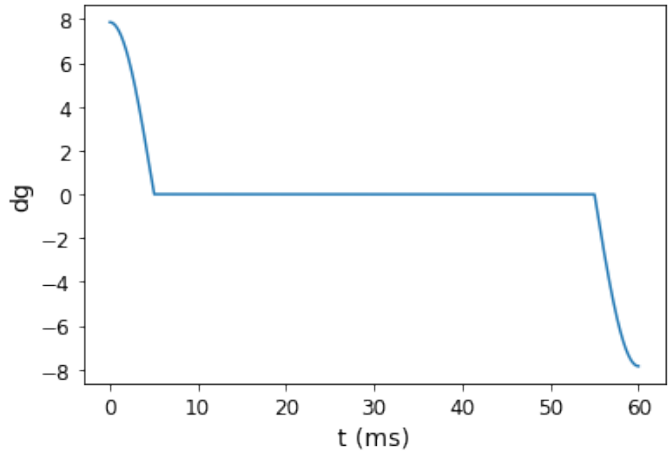

Figure 3.11: Time derivative of the Ramsey sensitivity $\frac{d}{dt}g(t)$ against time t for two 5 ms $\frac{\pi}{2}$ pulses and $T_d = 50$ ms

As there are two separate $\frac{\pi}{2}$ pulses, we are concerned with the front half of the first curve and the first half of the second curve. Since the first half of the second curve is very close to zero, its contribution to the change in excitation probability δp is very small. In effect, only the phase chirp induced by first $\frac{\pi}{2}$ pulse has a significant contribution.

3.3.3 Hyper-Ramsey Pulse

Yudin's Hyper-Ramsey[10] sequence ($\frac{\pi}{2} - T_d - \frac{3\pi}{2}$) has a sensitivity function similar to the Ramsey $g(t)$ derived above, but has five parts due to the two additional $\frac{\pi}{2}$ pulses after the dark time.

The simplest Bloch sphere representation of this sequence is a 2π rotation about the y-axis, with a precession about the z-axis due to the detuning during T_d. Extending the Ramsey sensitivity function with two more $\frac{\pi}{2}$ pulses, we derive the Hyper-Ramsey $g(t)$:

$$g(t) = \begin{cases} \sin\left(\frac{\pi}{2} \cdot \frac{t}{t_i}\right) & \text{for } 0 \leq t < t_i \\ 1 & \text{for } t_i \leq t < T_d + t_i \\ \cos\left(\frac{\pi}{2} \cdot \frac{t - T_d - t_i}{t_i}\right) & \text{for } T_d + t_i \leq t < T_d + 2t_i \\ -\sin\left(\frac{\pi}{2} \cdot \frac{t - T_d - 2t_i}{t_i}\right) & \text{for } T_d + 2t_i \leq t < T_d + 3t_i \\ \cos\left(\frac{\pi}{2} \cdot \frac{t - T_d - 3t_i}{t_i}\right) & \text{for } T_d + 3t_i \leq t < T_d + 4t_i \end{cases} \tag{3.26}$$

The plot of the Hyper-Ramsey $g(t)$ against time t is:

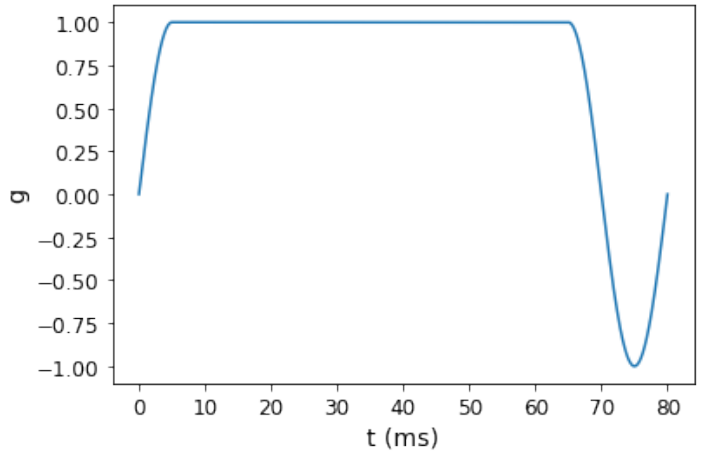

Figure 3.12: Hyper-Ramsey sensitivity $g(t)$ against time t for four 5 ms $\frac{\pi}{2}$ pulses and $T_d = 50$ ms

Its time derivative is:

$$\frac{d}{dt}g(t) = \begin{cases} \frac{\pi}{2t_i}\cos\left(\frac{\pi}{2}\cdot\frac{t}{t_i}\right) & \text{for } 0 \le t < t_i \\ 0 & \text{for } t_i \le t < T_d + t_i \\ -\frac{\pi}{2t_i}\sin\left(\frac{\pi}{2}\cdot\frac{t-T_d-t_i}{t_i}\right) & \text{for } T_d + t_i \le t < T_d + 2t_i \\ -\frac{\pi}{2t_i}\cos\left(\frac{\pi}{2}\cdot\frac{t-T_d-2t_i}{t_i}\right) & \text{for } T_d + 2t_i \le t < T_d + 3t_i \\ \frac{\pi}{2t_i}\cos\left(\frac{\pi}{2}\cdot\frac{t-T_d-3t_i}{t_i}\right) & \text{for } T_d + 3t_i \le t < T_d + 4t_i \end{cases} \tag{3.27}$$

And the plot of $\frac{d}{dt}g(t)$ against time t is:

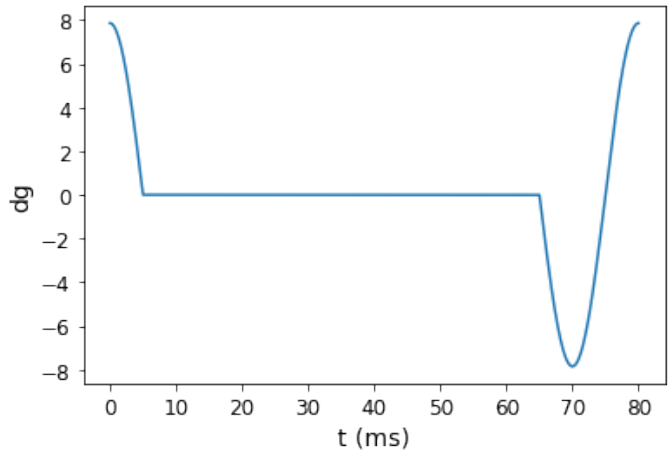

Figure 3.13: Time derivative of the Hyper-Ramsey sensitivity $\frac{d}{dt}g(t)$ against time t for four 5 ms $\frac{\pi}{2}$ pulses and $T_d = 60$ ms

An alternative proposal by Falke et. al.[9] is the inclusion of two short dead times between the three $\frac{\pi}{2}$ pulses to reset the optical path length stabilisation. If the phase chirp is the same for all four $\frac{\pi}{2}$ pulses, the chirp effect will effectively be cancelled out by its integral with the sensitivity function.

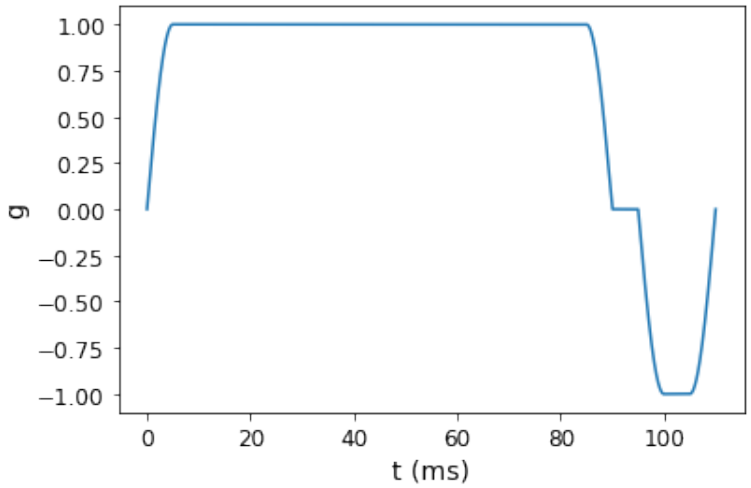

Figure 3.14: Falke's proposed Hyper-Ramsey scheme that includes two short dark times between the three $\frac{\pi}{2}$ pulses towards the end

This can be seen from the shape of sensitivity function in Figure 3.13 - phase chirp effect from the first pulse cancels out with the third, and that from the second pulse cancels out with the fourth.

4. Experiment

This chapter gives a description of the experimental setup and explains how phase chirps are measured.

4.1 Setup

A schematic diagram of the experiment is shown below:

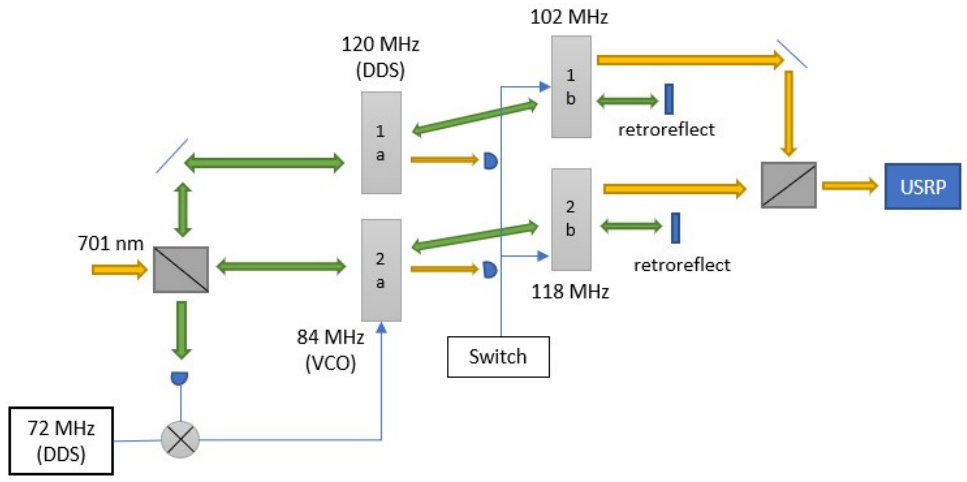

Figure 4.1: Schematic of the experimental setup. The green path is phase stabilised, while the yellow path is not.

There are two Michelson interferometers in this setup: one for path length stabilisation, and the other for phase measurement. Phase stabilisation involves the first pair of AOMs (1a & 2a) and the retro-reflective mirrors, while phase measurement involves the second pair of AOMs (2a & 2b), which are digitally switched by a computer.

From the left of Figure 4.1, the 701 nm laser is split into two paths by a beamsplitter. Only the first order diffracted beams from the first pair of AOMs are passed into the second pair of AOMs. The zeroth order beams at that point are reflected back unto the same path and beat at the first beamsplitter.

Since the retroreflected light passes through the first pair of AOMs twice, the beat signal produced has a frequency twice of their difference (i.e. $(120 - 84) \times 2 = 72$ MHz). This beat

signal is then mixed with an external 72 MHz signal by a direct digital synthesiser (DDS) to produce an error signal due to path length deviations. This error signal is fed to VCO driving AOM 2a, and when phase lock is engaged, the VCO corrects the error accordingly to achieve path length stabilisation.

The optical path length stabilization ensures a constant phase difference from the laser up to the second pair of AOMs (1b and 2b). Hence, only the optical paths after the second pair of AOMs can cause phase shifts. This is important in isolating the second pair of AOMs for the measurement of phase chirps due to switching.

The first order diffracted beams from the second pair of AOMs beat at a second beamsplitter to give an approximately 20 MHz (i.e. $120 + 102 - 118 - 84$ MHz) signal and enters the USRP. There, the beat signal is mixed with the USRP's 20 MHz signal. The difference between the two signals gives us a phase difference based on IQ demodulation, and any change in this difference must be due to switching of the second pair of AOMs.

4.2 Benchmark

For this experiment, an in-house laser of wavelength 701 nm is used, powered at by a current of 79.5 mA.

Each of the four AOMs is driven by an individual DDS board (MEL-0069v4) set at their respective frequencies from Python, and an amplifier (Mini-Circuits ZHL-1-2W-S) with appropriate RF power to diffraction efficiency (as given in the manual). Because the 120 MHz AOM is fed directly by the DDS, a smaller amplifier (Mini-Circuits ZHL-32-S) is used. The model for all the AOMs is ISOMET 1206C, with serial numbers starting with MT-0019. The 102 MHz AOM is set at a slightly lower frequency (-0.004656613 MHz) to match the USRP's coerced frequency.

Throughout the setup, neutral density (ND) filters were used to adjust the optical power of the laser for the longevity of the AOMs. Suitable lenses were also used to manage the beam waist before each AOM such that power loss is minimised.

5. Results

This chapter presents original results from the experiment and discusses their significance. Due to major renovations to the lab, the experiment was done in three periods with slightly different setups.

5.1 First Setup

The first setup in the lab was done by research assistant Yang Yuanhang, who first investigated the AOM chirp effect before passing the project to me.

5.1.1 RF Power of AOMs

The RF power driving an AOM can be reduced by adding attenuators in series. For this experiment, attenuators from 0 to 10 db (at increments of 1 db) are connected to the amplifier. Only one AOM (2b) is being switched. The amplitude and phase data for the chirp effect are arranged into single plots as shown below:

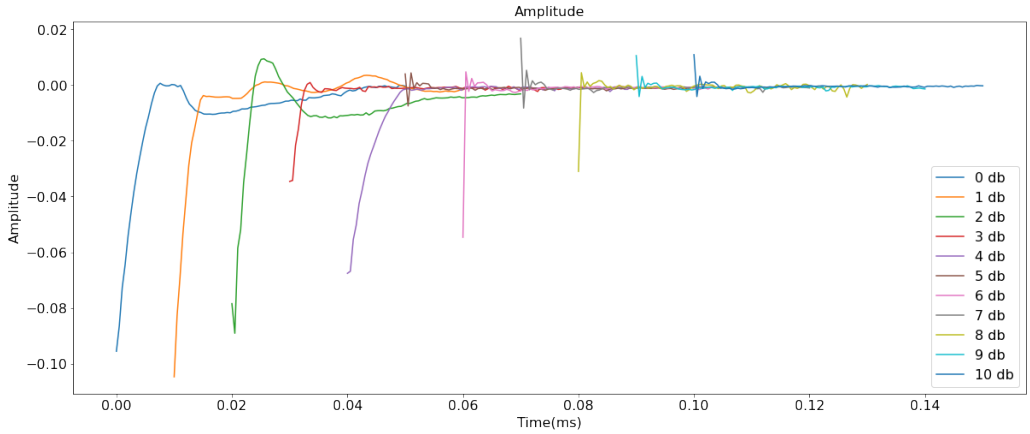

Figure 5.1: Plot of amplitude against time, with increasing attenuation from left to right

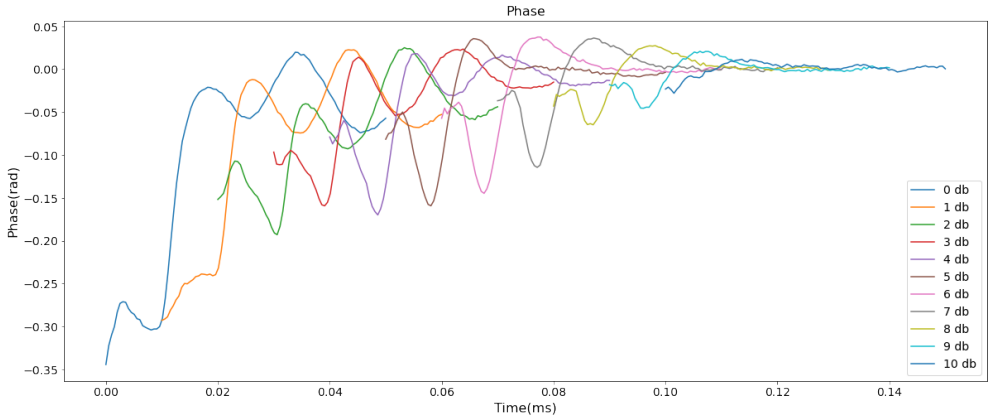

Figure 5.2: Plot of phase against time, with increasing attenuation from left to right

From Figure 5.2, it is apparent that the phase chirp effect diminishes as attenuation increases, or as RF power driving the switching AOM decreases. The frequency shifts for Rabi and Ramsey spectroscopy can then be numerically computed on Python by integrating the phase data with their respective sensitivity functions.

5.1.2 Type of Interrogation

For calculations, we use a Rabi π pulse of total interrogation time $T = 60$ ms. Relative to a clock frequency of 353 THz, the plot of frequency shift (Hz) against attenuation (db) is:

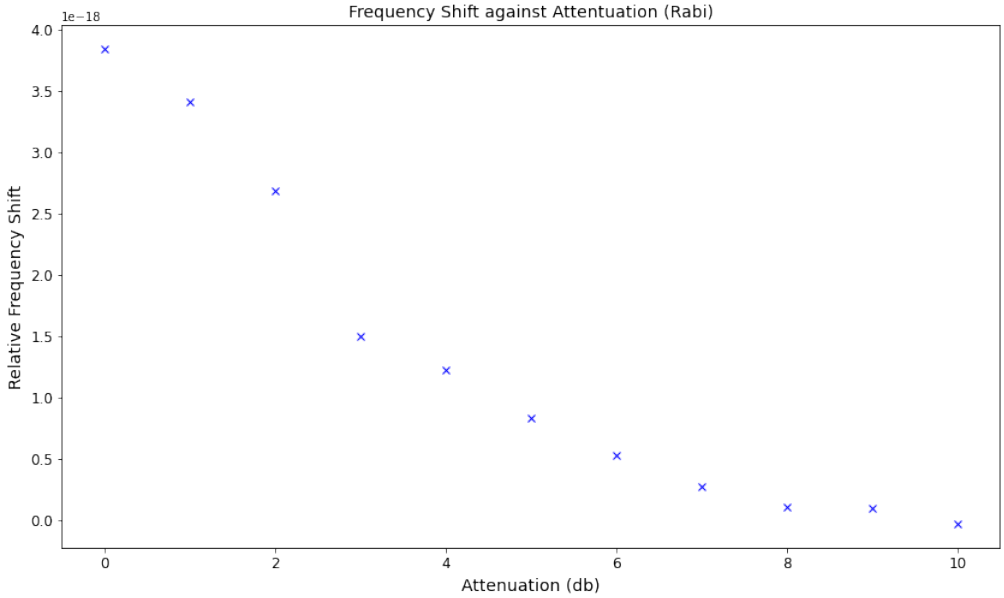

Figure 5.3: Frequency shift (Hz) against Attenuation (db) for a 60 ms Rabi π pulse

The plot shows a clear decrease in relative frequency shift with increasing attenuation (or decreasing RF power driving the AOM). At higher attenuations, the signal to noise ratio becomes much lower and background phase noise from the data dominates the chirp effect. This can be seen from the phase chirps for 8 to 10 db attenuation from Figure 5.2, where the wave forms are close to zero and barely distinguishable from the background phase data. As a result, their integrals with the sensitivity function gave negative values.

If we lengthen the interrogation time to 600 ms, the resulting frequency shifts are about 10 times smaller:

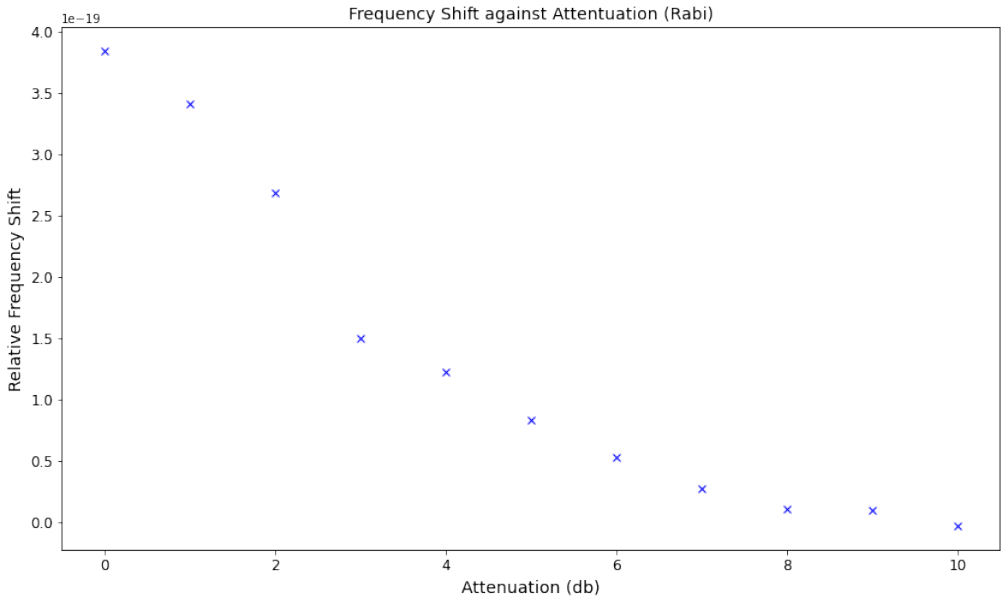

Figure 5.4: Frequency shift (Hz) against Attenuation (db) for a 200 ms Rabi π pulse

This means that as the Rabi interrogation time increases, the magnitude of the frequency shift due to a phase chirp from switching AOM decreases. This is an expected result because the frequency shift is proportional to the FWHM, which is twice of the HWHM (Equation 3.19). Since the HWHM of Rabi spectroscopy is inversely proportional to the interrogation time T (Equation 3.12), the frequency shift decreases as T increases.

For a Ramsey $\frac{\pi}{2} - T_d - \frac{\pi}{2}$ pulse, we set the pulse time $t_i = 5$ ms and the dead time $T_d = 50$ ms. Relative to a clock frequency of 353 THz, the plot of frequency shift (Hz) against attenuation (db) is:

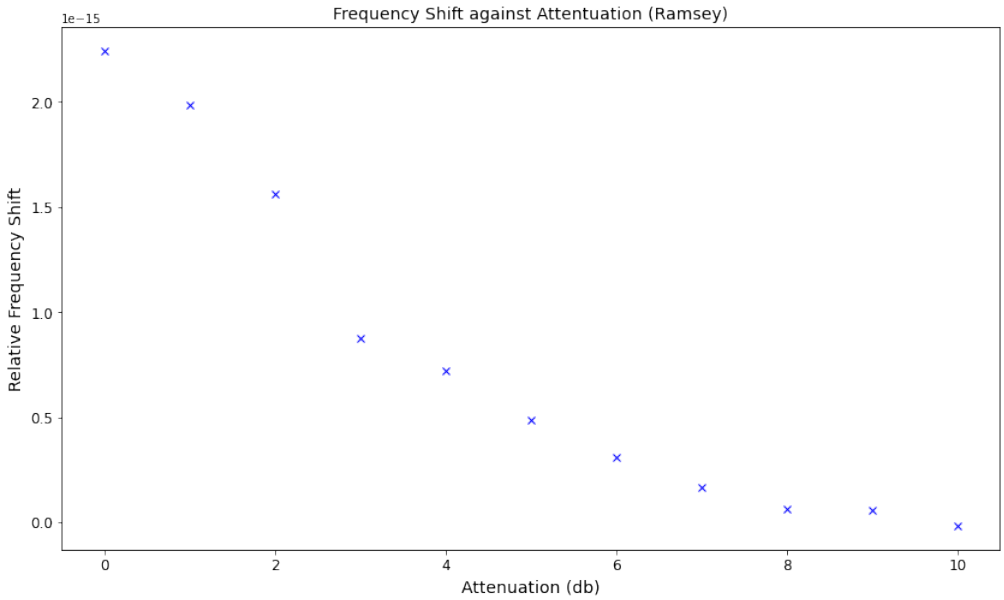

Figure 5.5: Frequency shift (Hz) against Attenuation (db) for a 60 ms Ramsey $\frac{\pi}{2} - T_d - \frac{\pi}{2}$ pulse

If we increase the pulse time t_i to 100 ms while keeping the dead time T_d the same at 50 ms, the resulting frequency shifts decrease in magnitude:

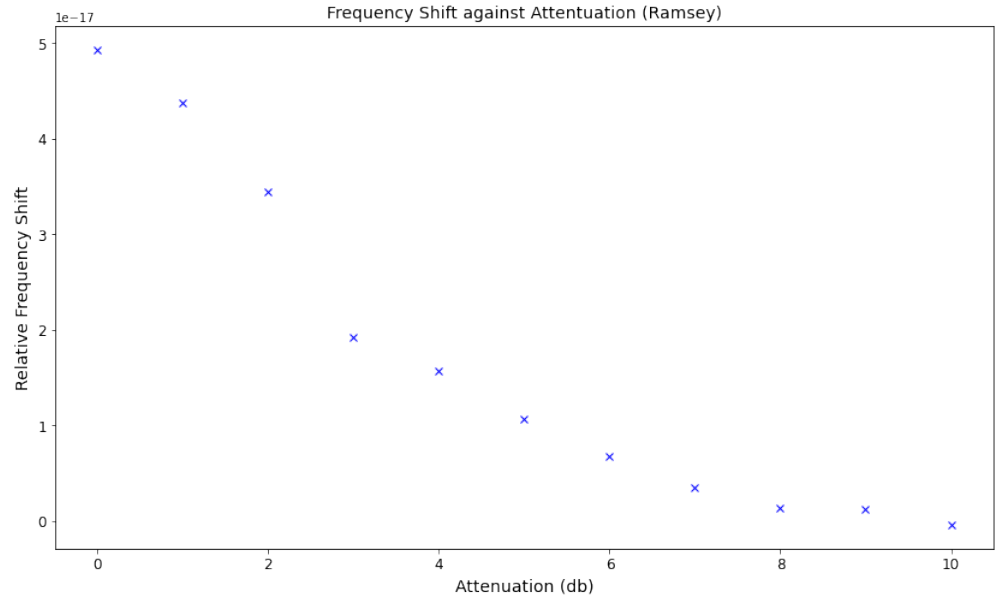

Figure 5.6: Frequency shift (Hz) against Attenuation (db) for a 250 ms Ramsey $\frac{\pi}{2} - T_d - \frac{\pi}{2}$ pulse

Since the chirp effect is only about $t = 0.05$ ms, the fraction of the total interrogation

time that includes the chirp decreases. Increasing t_i (or decreasing T_d) effectively makes the Ramsey sequence more Rabi-like. In fact, by setting $t_i = 30$ ms and $T_d = 0$ ms, we retrieve the exact same results as Figure 5.3.

If we keep the pulse time t_i at 5 ms and lengthen the dead time T_d to 240 ms, the resulting frequency shifts also decrease in magnitude:

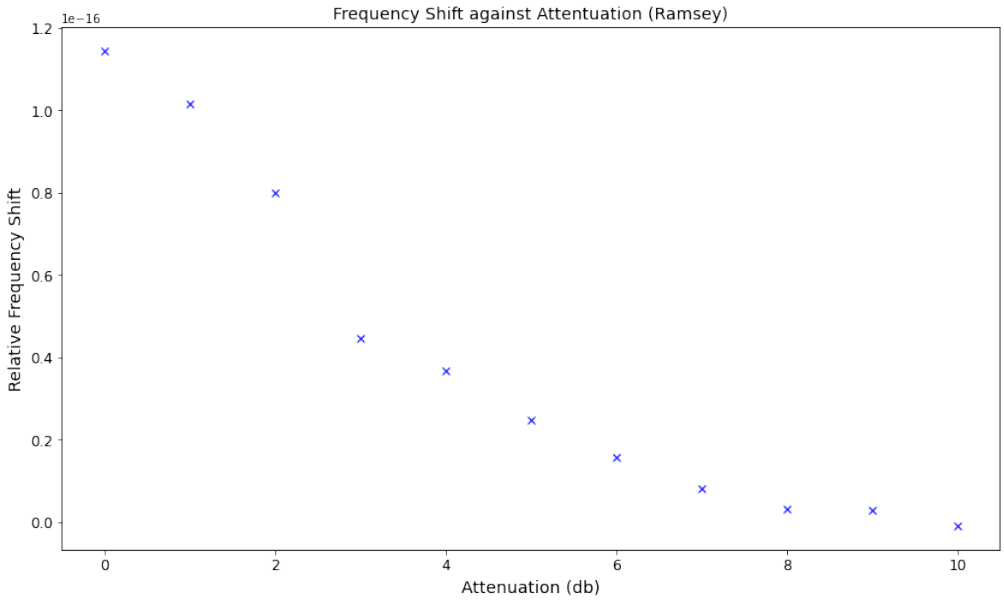

Figure 5.7: Frequency shift (Hz) against Attenuation (db) for a 250 ms Ramsey $\frac{\pi}{2} - T_d - \frac{\pi}{2}$ pulse

The frequency shifts decrease because the HWHM of Ramsey spectroscopy is inversely proportional to T_d (Equation 3.13). As T_d increases, the HWHM decreases, and since the frequency shift is directly proportional to the FHWM, the magnitude of frequency shifts decrease.

Note that the decrease in frequency shifts depends on the experimental parameters used. The above examples are meant to illustrate how we can manipulate interrogation time, pulse time, and dead time to reduce frequency shifts induced by phase chirps.

All graphs display a clear decrease in relative frequency shifts due to phase chirp as attenuation increases. Generally, the relative frequency shifts calculated for a typical Ramsey sequence are about 500 times greater than those for Rabi spectroscopy. Increasing interrogation time (T) for the Rabi sequence decrease relative frequency shifts. Increasing pulse time (t_i) and dead time (T_d) for the Ramsey sequence also decrease relative frequency shifts, although by experimental conventions the latter is preferred.

5.2 New Setup

As the air-con units in the lab were being replaced from late November to early February, the setup was shifted onto a portable breadboard and moved to the office. The same setup was replicated within the office with some changes in the optics used based on availability. Due to the lack of vibration isolation in the office, significant phase noise from the environment greatly diminished the visibility of the phase chirp effect. Nevertheless, analysing the phase data gave us some insights on how sensitive the setup is to environmental noises.

5.2.1 Improvements to Setup

The first improvement was to fix the polarisation of the laser to a vertical position from the start. In the pre-renovation setup, the laser was passed through an optical isolator with diagonal polarisation. While the polarisation of the laser is changed to vertical with a half-wave plate later in the setup, reflecting 45° polarisation with mirrors introduces an additional phase difference between its vertical and horizontal components. In order to remove this phase scrambling, the optical isolator was adjusted to a vertical polarisation before any reflection occurs.

The second improvement was to control the beam waist to maximise optical power of laser out of the AOMs. According to the ISOMET 1206C AOM datasheet[1], the optimal beam waist for 80% diffraction efficiency is 0.1 mm. Collimating lenses were placed in front of all AOMs so that the beam waist can be maintained at 0.1 mm before entry.

5.2.2 Characterising Phase Noise

Due to the lack of vibration isolation of the office table, the setup in the office was susceptible to phase noise from passive vibration from the environment. Passive vibration of the setup causes deviations in path length differences for both interferometers, and are amplified if the vibration is close to the resonant frequencies of the optics and the breadboard. As such, phase stabilisation could not be properly engaged and the phase chirp effect was washed out by these passive noises. Nevertheless, we thought it would be useful to characterise the passive noise in the office and how it contributes to the setup.

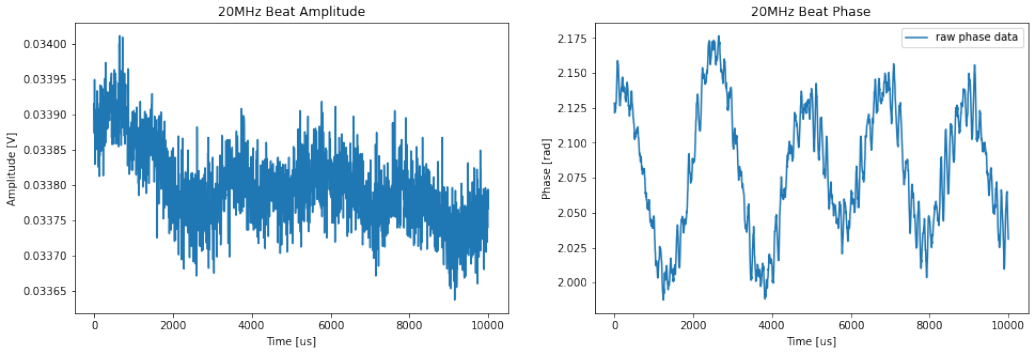

Figure 5.8: Amplitude and phase data in the office for 50 ms, without switching of AOMs

From phase data of Figure 5.8, there seems to be a phase oscillation of 0.09 radians at about 250 Hz. Besides, there are small oscillations in phase that correspond to higher frequencies. To identify these higher frequencies, we can do a discrete Fourier transform of the phase data from temporal to frequency basis. This was done by Welch's method[4], which estimates the power spectral density of a signal at different frequencies. Python has a convenient function that allows us to directly plot the Welch estimate with respect to the frequency of oscillations within the phase data. A phase data of 1 minute is used to improve the accuracy of the characterisation.

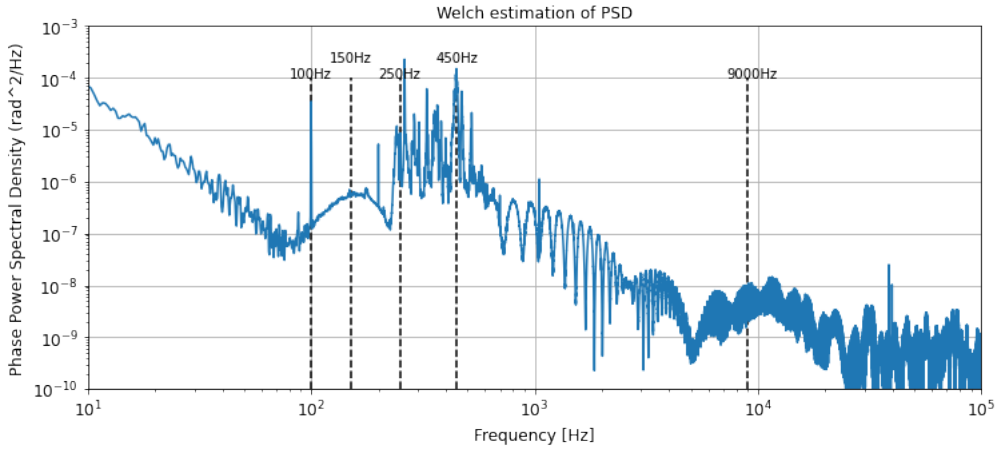

Figure 5.9: Welch estimate of phase data for 1 minute

From Figure 5.9, the Welch estimate shows notable peaks in 100 Hz and within the 250 to 450 Hz region. Phase noises in this frequency range are likely to be acoustic, which pertains the resonant frequencies of the optics in the setup.

To eliminate the possibility of electrical noises, the breadboard supporting the setup and

electric connections from the AOM amplifiers were grounded with grounding wires. Alas, no visible improvements was seen after grounding.

Another possibility we considered is to switch out VCO driving the 84 MHz AOM to driving the AOM directly with the DDS. The reason is that since the phase data we were taking were about 5 ms long, the short-term phase drift incurred by the lack of phase lock could be negligible. Effectively, this means removing the phase lock mechanism to see if its removal reduces the phase noise washing out the AOM chirp.

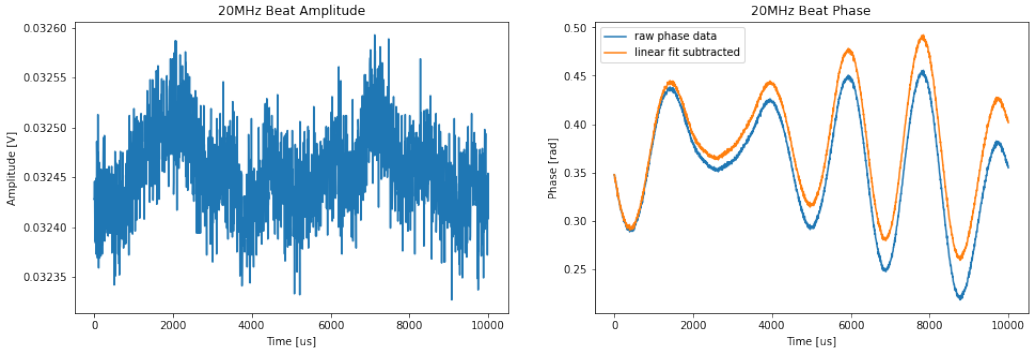

Figure 5.10: Amplitude and phase data in the office for 50 ms, without the phase lock mechanism

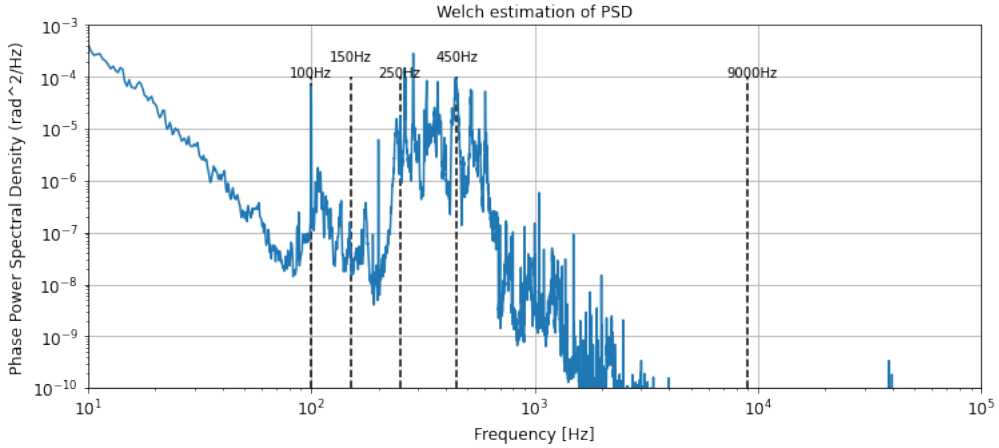

Figure 5.11: Welch estimate of phase data for 1 minute, without phase lock

Comparing Figure 5.9 and 5.11, we can see that the noise around the 9000 Hz region has diminished greatly, but the noise at 100 Hz, 250 to 450 Hz range still exists. This means that although removing the phase lock mechanism reduces phase noise at higher frequencies, it did not remove the significant phase noise washing out the AOM chirp.

5.3 Post-renovation

On early February, the setup was moved back to the lab and placed on an optical table. After realigning optics, the first task was to see whether the 100 Hz and 250 - 450 Hz phase noise disappears. Taking the amplitude and phase data for 50 ms:

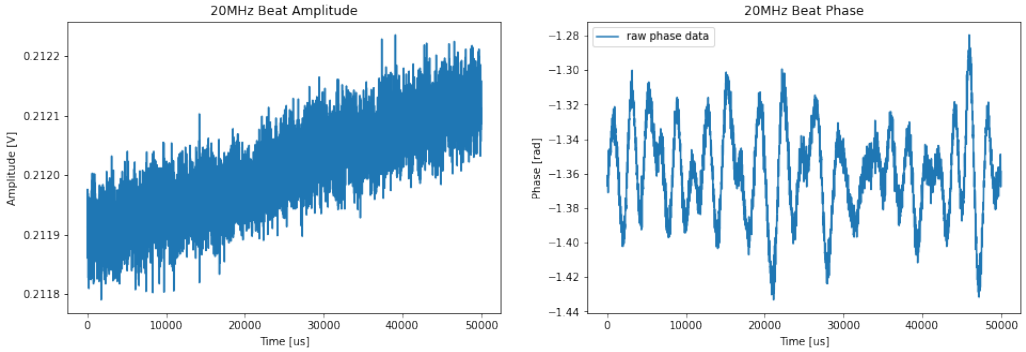

Figure 5.12: Amplitude and phase data for 50 ms in the lab after renovation, without switching of AOMs

Performing the Welch estimate once again on a 1 minute phase data and comparing it to the office setup:

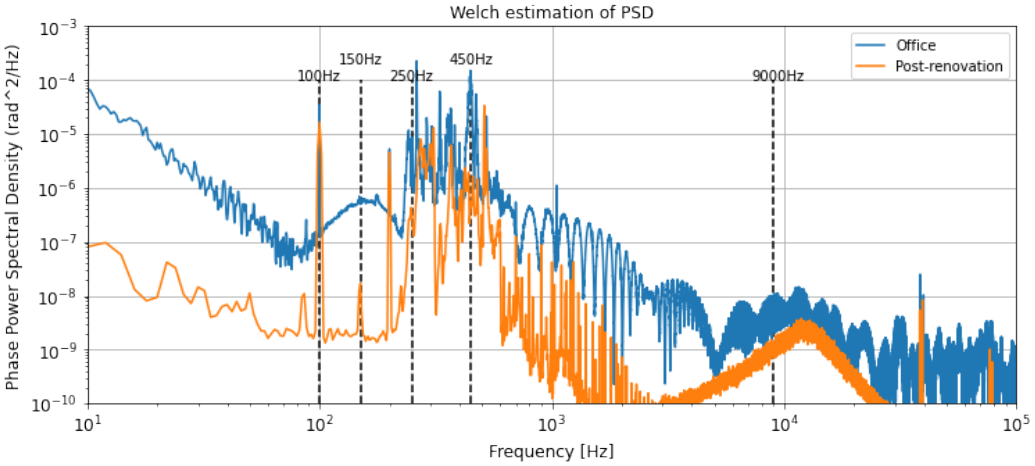

Figure 5.13: Welch estimate of phase data for 1 minute, with the setup before and after renovation

We can see from Figure 5.13 that while the phase power spectral density has decreased in magnitude across all frequencies, the phase noise in the 100 Hz, 250 - 450 Hz range still exists. This means that the passive vibration in the office was not the prime contribution of

phase noise, but could be related to the optics we were using and the breadboard they were attached to, or the electronics we were using in the lab.

5.3.1 More Improvements

The next step we thought of was to locate the resonant frequencies of the setup in the 250 - 400 MHz range, so that we can better guess which materials are responding most to passive vibrations. To do this, we placed a speaker beside the setup and played sounds at 50 Hz intervals from 200 to 700 Hz.

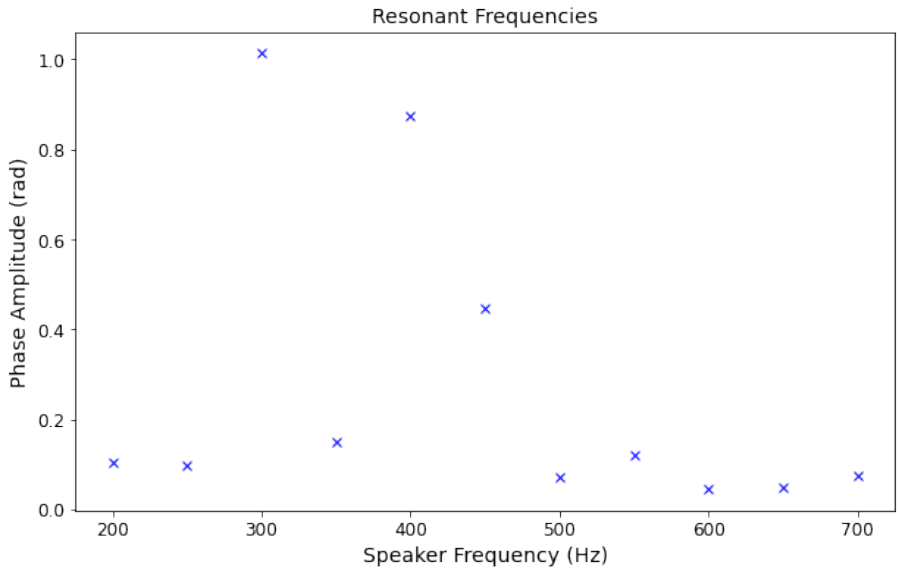

Figure 5.14: Plot of the mean phase amplitude against speaker frequency

From Figure 5.14, we can see that the setup responds most to the 300 Hz sound, followed by 400 MHz and 450 MHz. These frequencies are commonly associated with passive vibrations of the optics on the breadboard. In light of that, we made three minor adjustments to the setup.

First, we removed the supports under the breadboard and clamp it down to the optical table on all sides. We suspected that the air gap between the surface of the optical table and the underside of the breadboard could contribute passive vibration from slight changes in air pressure around the setup.

The second adjustment was to replace the mounts of the retroreflecting mirrors to more stable ones. This was to ensure that the phase lock mechanism is insensitive to passive vibrations from the breadboard.

The third adjustment was to change the post of the beamsplitter before the photodetector capturing the 20 MHz beat signal to one without clamps. We suspected that the clamp was not holding the beamsplitter in position and was vibrating with the table.

Unfortunately, none of these adjustments made significant difference to the phase noise.

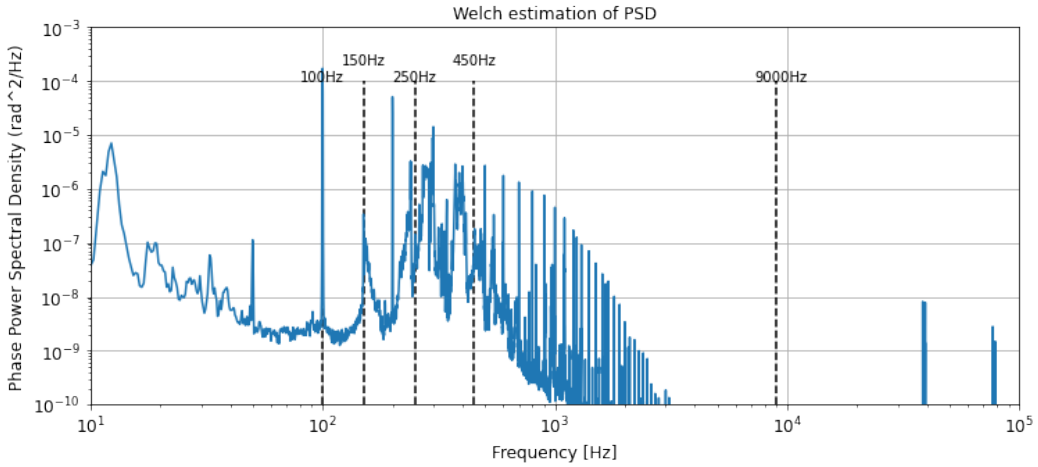

Figure 5.15: Welch estimate of 1 minute phase data after adjustments to the optics

The last adjustment we made was to change power supplies of the two photodetectors (one for the 72 MHz and the other for 20 MHz) to the same source. This was to eliminate the differences in grounding between the two photodetectors. Comparing the Welch estimate of the 1 minute phase data after these adjustments to the Welch estimate before:

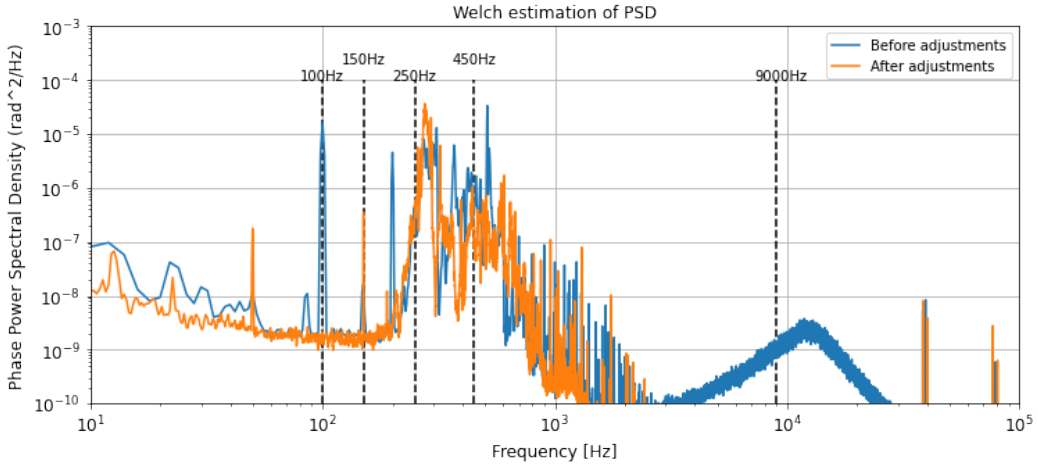

Figure 5.16: Welch estimate of 1 minute phase data before and after the minor adjustments to setup

While the 100 Hz phase noise seems to have disappeared, the noise within the 300 to 400 Hz range did not diminish. As the due date of the project was nearing, we tried to take the amplitude and phase data with increasing attenuation once again to see if the chirp effect can still be seen.

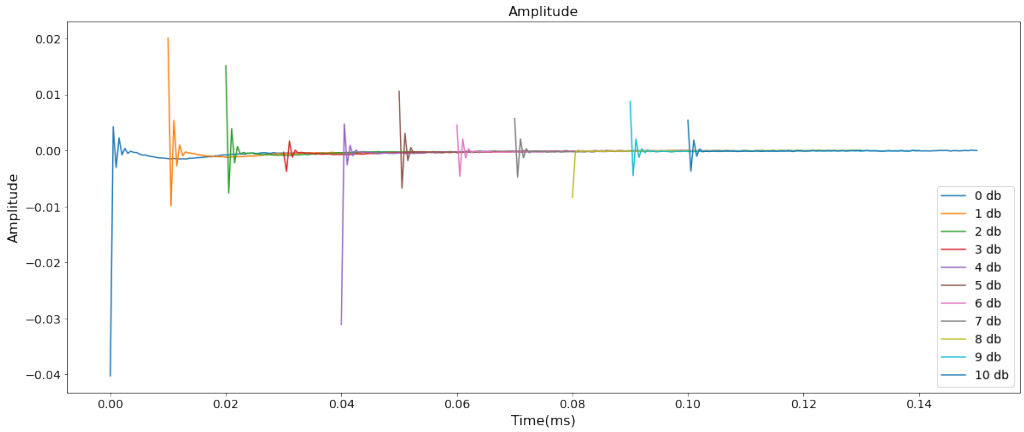

Figure 5.17: Plot of amplitude against time, with increasing attenuation from left to right

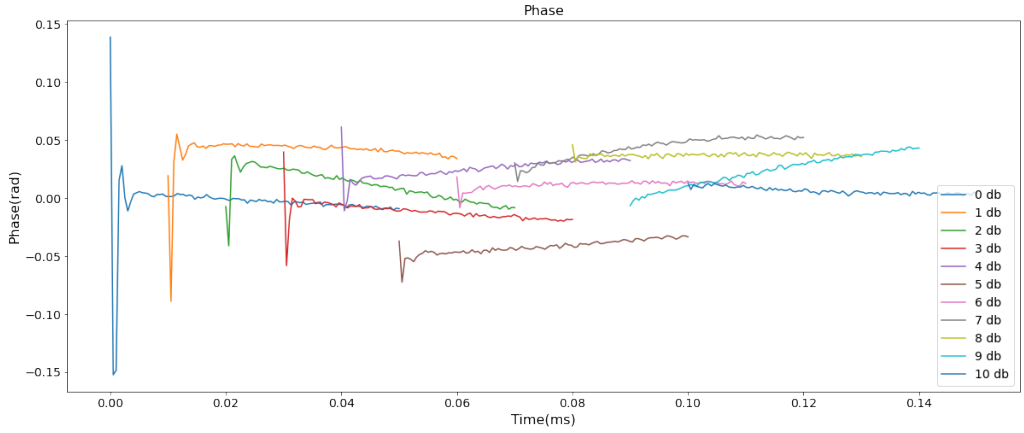

Figure 5.18: Plot of phase against time, with increasing attenuation from left to right

While the chirp effect is visibly decreasing with increasing attenuation, there is significant contribution of phase noise from the background that leads to phase drift after the chirp, despite having the phase lock engaged.

6. Conclusion

This work is part of an ongoing endeavour to characterise the phase chirp effects of switching AOMs. From Falke's initial findings[9], the relative frequency shift due to this phase chirp is below 2×10^{-17}, which is a significant consideration for our group in achieving 10^{-19} precision. Since the AOM is used to switch lasers for pulsed interrogation during clock operation and to compensate for path length changes by frequency shifts, it is important for us to understand how much error it could induce and what the main contributors of the phase shifts are.

From the initial setup done up by previous lab members, we were able to confirm that decreasing the RF power driving an AOM decreases the relative frequency shifts due to phase chirps from switching the AOM. While the magnitude of relative frequency shifts depends on the parameters of the interrogation techniques, we conclude that relative frequency shifts from Ramsey sequence were significantly higher than those from the Rabi sequence.

Due to major renovation works in the lab, the setup had to be relocated to an area without passive vibration isolation. Unfortunately, the new setup was susceptible to phase noise from the surroundings. Nevertheless, we managed to characterise the phase noise to some extent. First, we found that majority of the phase noise are from the 100 Hz, 250 to 450 Hz range. We further narrowed now this range to 300 to 400 Hz by sampling the resonant frequencies of the setup. Second, removing the phase lock mechanism by driving the 84 MHz AOM with DDS directly eliminates phase noise at higher frequencies, but it did not significantly reduce the phase noise obscuring the chirp effect. Third, subsequent adjustments made to the optics and power sources of the photodetectors reduced phase noise at 100 Hz, but there was no noticeable reduction of noise in the 300 to 400 Hz range.

6.1 Future Work

More work in finding out the sources of phase noise in the 300 to 400 Hz range is needed. One suggestion is to test the extent to which changes in air pressure around the setup could cause changes in phase of the beat signals. During our troubleshooting, we saw that the phase data responds significantly to speech, which momentarily changes air pressure in the

environment. As the refractive index of air n is associated with air pressure p by $n = 1 + kp$, where k is a constant of proportionality, an increase in p results in an increase in n, which means the speed of light travelling through air within the setup decreases. If wavelength of the laser remains relatively constant, a decrease in speed would mean a decrease in frequency. Since frequency is the derivative of phase with respect to time, a decrease in frequency due to air pressure would present itself as background phase noise.

Another suggestion is to sample the phase data of the optics we used on the same breadboard. This is to see how significantly the optics are contributing to the phase noise we see. The test can be done by setting up the laser to a mirror, then directly to a photodetector while keeping distances between the optics minimal. In addition, we could make a similar test setup on an optics table without the breadboard, and compare the phase data of the two tests to see if the breadboard was contributing significantly to the phase noise.

Lastly, once the phase noise is no longer obscuring the phase chirp, different models of AOMs could be used to check for any device dependencies of the chirp effect. This could be done by repeating the same experimental process we had for the first setup, except with the four AOMs changed out. Differences in phase chirp profiles between the two experiments would allow us to infer the possible mechanisms of the phase chirp effect within an AOM.

A. Excitation-related Shifts in Hyper-Ramsey

To see how the Hyper-Ramsey sequence eliminates excitation-related shifts, we start by expressing the probability of finding the atom in the excited state n_e as a Taylor expansion of $T_d\Delta$:

$$P(e) = a^{(0)} + a^{(1)}(T_d\Delta) + a^{(2)}(T_d\Delta)^2 + ... \tag{A.1}$$

where T_d is the dark time and Δ is the detuning of the laser. The coefficients of $T_d\Delta$ can be expanded as odd and even powers of $\frac{\delta}{\Omega_0}$:

$$\begin{aligned} a^{(0)} &= A_0^{(0)} + A_2^{(0)}(\frac{\delta}{\Omega_0})^2 + A_4^{(0)}(\frac{\delta}{\Omega_0})^4 + ... \\ a^{(1)} &= A_1^{(1)}(\frac{\delta}{\Omega_0}) + A_3^{(1)}(\frac{\delta}{\Omega_0})^3 + ... \\ a^{(2)} &= A_0^{(2)} + A_2^{(2)}(\frac{\delta}{\Omega_0})^2 + A_4^{(2)}(\frac{\delta}{\Omega_0})^4 + ... \end{aligned} \tag{A.2}$$

where δ is the effective frequency shift during the pulse (due to excitation-related shifts) and Ω_0 is the Rabi frequency. This is due to the symmetry of $P(e)$, which does not change when $\Delta \to -\Delta$ and $\delta \to -\delta$. Assuming that the effective frequency shift is small compared to the Rabi frequency ($|\frac{\Delta}{\Omega_0}| << 1$) and $|T_d\Delta| << 1$, we can approximate the shift of the central Ramsey fringe $\delta\omega_0$ as:

$$\begin{aligned} \delta\omega_0 &\approx -\frac{1}{T_d}\frac{a^{(1)}}{2a^{(2)}}\frac{\delta}{\Omega_0} \\ &= -\frac{1}{T_d}\frac{A_1^{(1)}}{2A_0^{(2)}}\frac{\delta}{\Omega_0} \end{aligned} \tag{A.3}$$

For a Ramsey sequence with two $\frac{\pi}{2}$ pulses, $\delta\omega_0$ gives a linear dependence on $\frac{\delta}{\Omega_0}$:

$$\delta\omega_0 = -\frac{1}{T_d}\frac{2\Omega_0 T}{2+\Omega_0 T}\frac{\delta}{\Omega_0} \tag{A.4}$$

It is possible to reduce the linear dependence of $\delta\omega_0$ to a cubic dependence. This can be

done by finding the condition such that the coefficient of the linear dependence $A_1^{(1)} = 0$. Solving $A_1^{(1)}$ analytically gives us:

$$A_1^{(1)} \propto sin[\Omega_0 \frac{(t_1 + t_2)}{2}] \tag{A.5}$$

for the two separate $\frac{\pi}{2}$ pulses of duration t_1 and t_2. The condition for $A_1^{(1)} = 0$ is:

$$\Omega_0(t_1 + t_2) = 2n\pi \tag{A.6}$$

where $n = 1, 2, 3...$ For $n = 1$, the simplest way to achieve this condition is to include a π pulse before the second Ramsey $\frac{\pi}{2}$ pulse, such that $t_2 = 3t_1$. Equivalently, we could have a $\frac{\pi}{2}$ pulse, followed by three $\frac{\pi}{2}$ pulses.

With the coefficient of the linear dependence eliminated, the dominating dependence is:

$$\delta\omega_0 \approx -\frac{1}{T_d} \frac{A_3^{(1)}}{2A_0^{(2)}} (\frac{\delta}{\Omega_0})^3 \tag{A.7}$$

The cubic dependence on $\frac{\delta}{\Omega_0}$ also reduces the sensitivity of the shift to a small change in δ. To see this, we compare the plots of a linear and cubic relationship of $\delta\omega_0$ with $\frac{\delta}{\Omega_0}$:

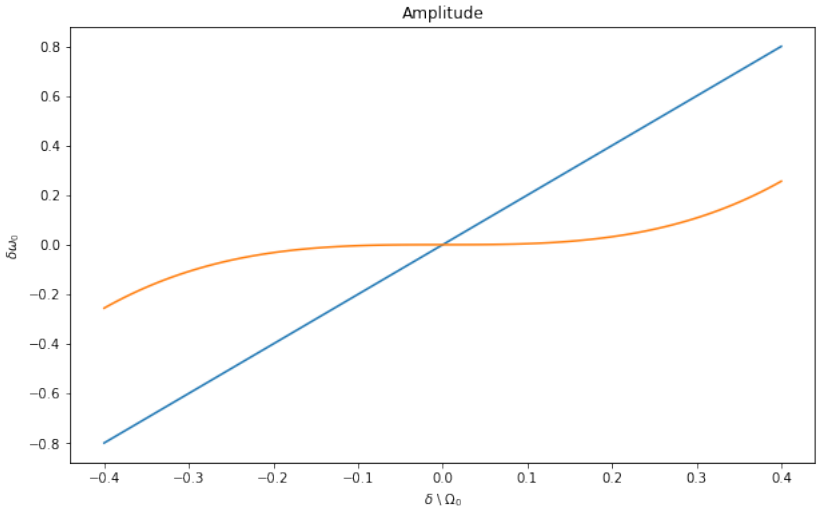

Figure A.1: Plot of a linear (blue) and cubic (yellow) dependence of $\delta\omega_0$ on $\frac{\delta}{\Omega_0}$

Around the point where $\frac{\delta}{\Omega_0} = 0$, the gradient of the cubic graph is much smaller than the gradient of the linear graph. This means that the Hyper-Ramsey sequence is much less

sensitive to small excitation-related shifts than the usual Ramsey sequence.

It should be noted that the additional π pulse in the Hyper-Ramsey sequence requires a phase jump of π, such that it can be seen as a pulse with $-\Omega_0$ in contrast to the other two $\frac{\pi}{2}$ pulses. This is because in some clocks, we cannot perfectly fulfill the condition given by equation (3.20), which reintroduces linear dependence on $\frac{\delta}{\Omega_0}$ in the two $\frac{\pi}{2}$ pulses. With the π phase jump, the linear dependence of the $\frac{\pi}{2}$ pulses is cancelled out by that of the π pulse.

Bibliography

[1] 1206C-833 Acousto-Optic Modulator, 2020. https://www.japanlaser.co.jp/wp-content/uploads/2020/02/1206C-833.pdf. Accessed 03 Apr 2022.

[2] D.J. McCarron. A Guide to Acousto-Optic Modulators, 2007. http://themccarrongroup.com/wp-content/uploads/2020/03/AOM-Guide.pdf. Accessed 03 Apr 2022.

[3] G. John Dick. Local Oscillator Induced Instabilities in Trapped Ion Frequency Standards. *Proceedings of 19th Annu. Precise Time and Time Interval Meeting, Redendo Beach (U.S. Naval Observatory, Washington)*, pages 133–147, 1987.

[4] J.O. Smith III. Welch's Method, 2022. https://ccrma.stanford.edu/~jos/sasp/Welch_s_Method.html. Accessed 03 Apr 2022.

[5] M.D. Barrett. PC4243 - Atomic and Molecular Physics II, 2020.

[6] R. Kaewuam, T. R. Tan, K. J. Arnold S. R. Chanu, Zhiqiang Zhang, M. D. Barrett. Hyperfine Averaging by Dynamic Decoupling in a Multi-Ion Lutetium Clock. *Physical Review Letters 124: 083202*, 2020. arXiv:1910.04983.

[7] Robert Keim. Understanding Quadrature Demodulation. https://www.allaboutcircuits.com/textbook/radio-frequency-analysis-design/radio-frequency-demodulation/understanding-quadrature-demodulation/. Accessed 03 Apr 2022.

[8] R.W. Gammon. The Michelson Interferometer, 2006. https://www.physics.umd.edu/courses/Phys375/GammonSpring06/lab4.pdf. Accessed 03 Apr 2022.

[9] S. Falke, M. Misera, U. Sterr, C. Lisdat. Delivering pulsed and phase stable light to atoms of an optical clock. *Applied Physics B - Lasers and Optics, Vol. 107*, pages 301 – 310, 2012. arXiv:1108.3729v2.

[10] V.I. Yudin, A. V. Taichenachev, C. W. Oates, Z. W. Barber, N. D. Lemke, A. D. Ludlow, U. Sterr, Ch. Lisdat, F. Riehle. Hyper-ramsey spectroscopy of optical clock

transitions. *The American Physical Society. Rapid Communications, Physical Review A 82, 011804*, 2010.

[11] Zhang Zhiqiang, K. J. Arnold, R. Kaewuam, M. S. Safronova, M. D. Barrett. Hyperfine-mediated effects in a Lu+ optical clock. *Phys. Rev. A 102, 052834*, 2020. arXiv:2009.02889.